ACS Sustainable Chemistry & Engineering

pubs.acs.org/journal/ascecg

Research Article

Dispensing Essential Oil Components through Cocrystallization: Sustainable and Smart Materials for Food Preservation and Agricultural Applications

Fabio Montisci, Paolo P. Mazzeo,* Claudia Carraro, Michele Prencipe, Paolo Pelagatti, Fabio Fornari, Federica Bianchi, Maria Careri, and Alessia Bacchi*

Cite This: *ACS Sustainable Chem. Eng.* 2022, 10, 8388−8399

Read Online

ACCESS | Metrics & More | Article Recommendations | Supporting Information

ABSTRACT: The ever-increasing attention on environmental problems and sustainability has highlighted several problems related to the use of conventional pesticides in the agricultural industry, e.g., toxic residues in the soil and hazards to the environment and human health. In the search for natural antimicrobial and insecticide alternatives, essential oils (EOs) and their active components have emerged as promising candidates, but they suffer from some drawbacks related to their physical properties. We exploited cocrystallization with isonicotinamide, pyrazine, 2,3,5,6-tetramethylpyrazine, and 2,3-dimethylquinoxaline as a workaround to extend the applicability of carvacrol and thymol as natural pesticides, improving their ambient delivery profile. The cocrystals were prepared mechanochemically in a green solvent-free manner, and their purity, structure, and stability were investigated via powder and single-crystal X-ray diffraction (XRD), differential scanning calorimetry (DSC), thermogravimetric analysis (TGA), and density functional theory (DFT) calculations. Moreover, each cocrystal was also tested in terms of EO release by headspace−gas chromatography−mass spectrometry (GC−MS) analysis over 14 days. We also report the conversion of a cocrystal to a new structure with different stoichiometry, which seems to afford a delayed boost of EO release that could be very interesting for food preservation applications.

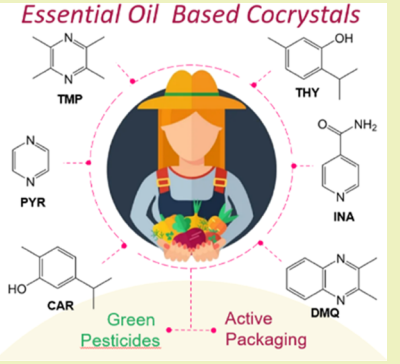

KEYWORDS: *cocrystals, essential oils, crystal engineering, mechanochemistry, controlled release, natural pesticides, food preservation*

INTRODUCTION

Lowering the impact of industrial activities on the planet's environment is one of the most pressing concerns of our time and is increasingly gaining traction in humankind's awareness. For the agricultural sector, this has translated into the recognition that conventional chemical treatments for weed, pest, and disease control present several problematic aspects, ranging from the deposit of toxic residues in the soil[1] to concerns for the environment and human health.[2,3] As a response, in the last few decades, we have seen a strive to develop safer and more sustainable methods to replace conventional pesticides.[4,5]

One of the most promising classes of compounds that can act as natural pesticides is that of essential oils (EOs), substances produced from plants as secondary metabolites with high content of terpenes, terpenoids, and aromatic compounds. EOs have been shown to have antibacterial, antiviral, antifungal, and insecticide effects,[6−8] and they have also been considered for many other applications such as pharmaceuticals, alternative medicine, natural therapies, and especially food preservation.[7−11]

Reducing food waste is another crucial objective in the quest for sustainability, and many efforts have been made to extend food shelf life.[11,12] Active packaging, in which the food preservatives are directly incorporated into the packaging system, is a very promising technology, presenting the double advantage of a decreased amount of required active substance and the possibility of avoiding direct contact with food during processing.[13−16] Thanks to their antimicrobial properties and the fact that they are classified as "Generally Recognized As Safe" (GRAS) by the Food and Drug Administration,[17,18] EOs and their single active components have aroused interest to be used in active packaging as a replacement for synthetic additives that could be associated with adverse health effects.[15,19]

Even though the properties of the essential oils against parasites are well documented, their application in the agriculture and food industry is limited by their intrinsic complex composition, poor solubility in water, and high volatility. These aspects pose some difficulties for the exploitation of their antimicrobial properties both for plant

Received: March 2, 2022
Revised: June 2, 2022
Published: June 24, 2022

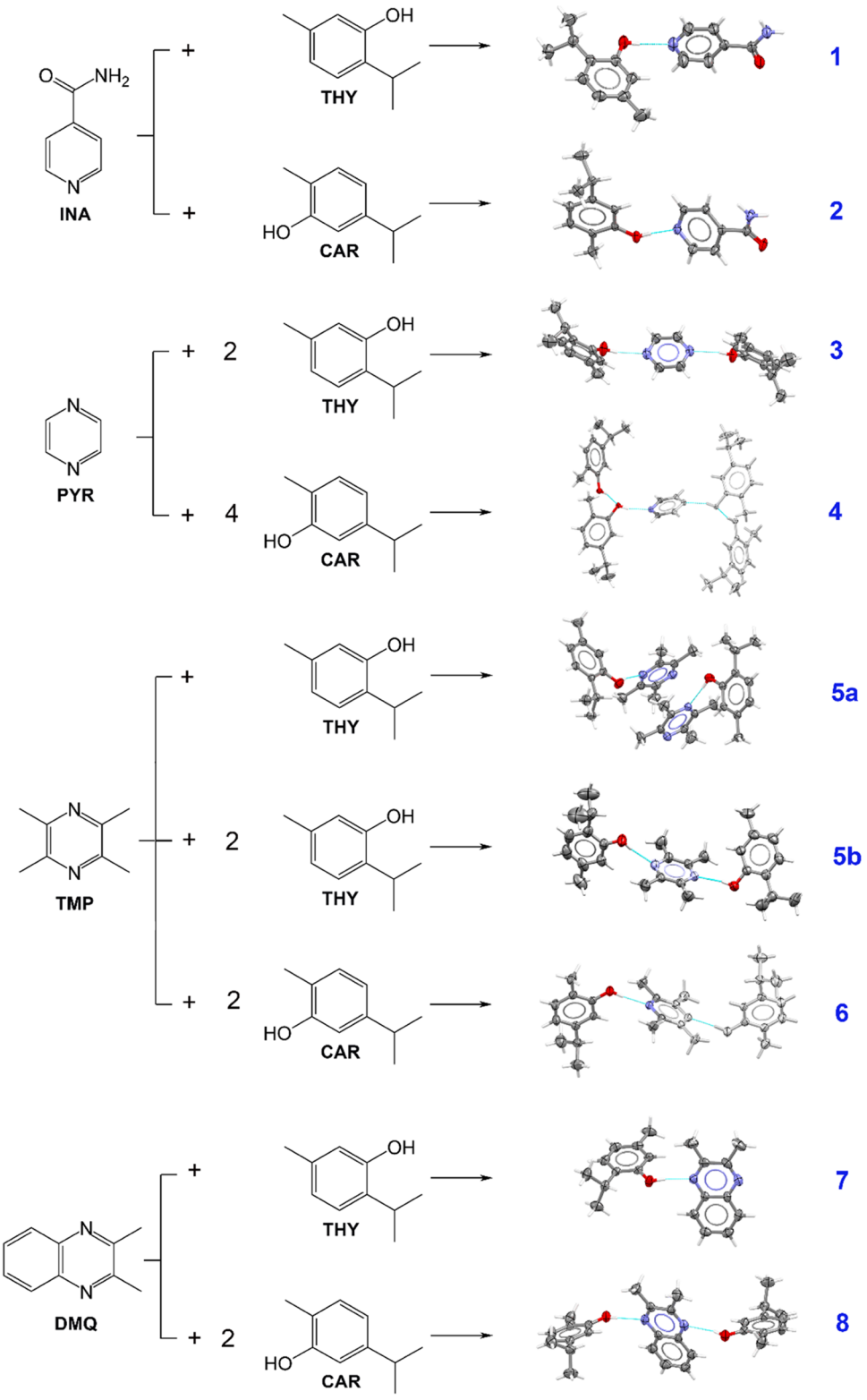

Figure 1. Schematic representation of the cocrystals **1**−**8** synthesized from the combination of two constituents of essential oils (THY = thymol and CAR = carvacrol) and four coformers (INA = isonicotinamide, PYR = pyrazine, TMP = 2,3,5,6-tetramethylpyrazine, and DMQ = 2,3-dimethylquinoxaline). Thumbnail of the corresponding crystalline structures showing the core EO-coformer assemblies. Color code: C = gray, N = blue, O = red H = white. All atoms outside the asymmetric unit are reported in white. Blue dotted lines represent intermolecular H-bonds.

protection in agriculture and for their integration in food packaging, which need to be addressed with new formulations of these compounds.[20,21]

Crystal engineering is a branch of solid-state chemistry that aims at building up functional crystalline materials by combining different molecular entities within the same crystal structure.[22−30] What emerges from a crystal engineering approach is

https://doi.org/10.1021/acssuschemeng.2c01257
ACS Sustainable Chem. Eng. 2022, 10, 8388−8399

that the ultimate properties of the resulting material depend on the way molecules are arranged in the solid state and on the intermolecular interactions established among chemical entities. Cocrystals are single-phase crystalline materials composed of different chemical entities in a stoichiometric ratio. They have been widely explored in the field of crystal engineering,[31−35] and they have found significant pharmaceutical applications,[36,37] although they have appeared only sporadically in the environmental-related literature.[38−41] In recent publications, we highlighted how cocrystallization can be an especially viable solution to this problem, allowing us to tune the physical properties and control the delivery of EOs components, thus extending their range of applicability.[11,41−43]

Although most cocrystals reported in the literature are prepared from solid reagents,[44] cocrystal syntheses in which liquid components are involved are also possible,[41,45−48] providing a great way to stabilize the liquid ingredient in a solid form and generally improving its stability and simplifying their storage and handling.[45] By leveraging our knowledge of the possible supramolecular interactions between different compounds, it is possible to select appropriate molecular partners (i.e., coformers) to create a network of intermolecular interactions capable to stabilize a liquid or low melting compound into a crystalline form.[32,34,36,49,50] Moreover, since the crystal structure of a material is responsible not only for thermal stability but also for many other properties (e.g., solubility, hygroscopicity, density, mechanical strength, etc.[51−53]), the expert engineering of cocrystals can offer a way to create new materials which contain the desired ingredients with improved characteristics (e.g., better shelf life or performances).[32,51]

In this work, we present cocrystals of positional isomers carvacrol (CAR, extracted from oregano, liquid at room temperature)[54] and thymol (THY, the main component of thyme)[55] with enhanced release characteristics for applications as natural pesticides and food preservatives.[56] THY and CAR were chosen as active components due to their large usage and availability, as well as their known bioactivity against bacteria and fungi.[27,41,57] Recently, we have demonstrated the biological activity of THY and CAR against Gram-negative and Gram-positive bacteria and against in vitro fungal strains even when formulated as cocrystals with non-bioactive coformers.[41] In that work, phenazine and hexamethylenetetramine were considered as pilot coformers to develop a proof of concept. Here, we report on the GRAS−GRAS cocrystals with aromatic coformers containing a pyridinic nitrogen atom prone to interact strongly as a hydrogen-bond (HB) acceptor with the phenolic hydroxyl group of THY and CAR. Indeed, since the crystal structure of pure THY[58] is dominated by an HB network between hydroxyl groups (Figure S49), to further stabilize the molecule of interest in a new material, we need to select a molecular partner that can form even stronger interactions with it.

In the specific, we selected a coformer bearing an amidic group—isonicotinamide (INA)—and a family of coformers with pyridinic nitrogen and increasing molecular size—pyrazine (PYR), 2,3,5,6-tetramethylpyrazine (TMP), and 2,3-dimethylquinoxaline (DMQ)—to stabilize the active components THY and CAR and mitigate their acute release in favor of a more balanced release over time.

The combinations of all GRAS-EO/GRAS-coformer pairs (Figure 1 and Table 1) resulted in eight cocrystals having a possible advantage for the application in the agrochemical and food-related industry. All of the samples were synthesized by solvent-free mechanochemical procedures[59−61] such as manual grinding and ball milling. Providing a sustainable and cheaper strategy for synthesis compared with traditional solution methods, mechanochemistry was dubbed by the International Union of Pure and Applied Chemistry (IUPAC) among the 10 chemical innovations that will change our world.[62] Crystal structures of all cocrystals were determined via single-crystal X-ray diffraction (SCXRD), while the purity of the samples was checked by powder X-ray diffraction (PXRD). Their thermal behavior was characterized by differential scanning calorimetry (DSC) and thermogravimetric analysis (TGA). Intermolecular interaction energies in the crystal packing were computed with CrystalExplorer17 at the B3LYP/6-31g(d,p) level.

Table 1. List of Cocrystals with the Corresponding Numeric Label[a]

cocrystal	coformer	EO component	stoichiometry
1	INA	THY	1:1
2	INA	CAR	1:1
3	PYR	THY	1:2
4	PYR	CAR	1:4
5a	TMP	THY	1:1
5b	TMP	THY	1:2
6	TMP	CAR	1:2
7	DMQ	THY	1:1
8	DMQ	CAR	1:2

[a]THY = thymol, CAR = carvacrol, INA = isonicotinamide, PYR = pyrazine, TMP = 2,3,5,6-tetramethylpyrazine, and DMQ = 2,3-dimethylquinoxaline.

We showed how the combination with different coformers affects both the physical properties of each sample and the delivery profile of the EO component. In the present investigation, moreover, we studied the conversion of a cocrystal (i.e., **5a**) into another with different stoichiometry (i.e., **5b**), obtaining a product of potential interest for the development of active packaging materials.

EXPERIMENTAL SECTION

Synthesis of Cocrystals. Cocrystals **1**−**8** were prepared in bulk by manual neat grinding, with no need for any solvent to be added. The resulting powder samples were collected in closed vials. Single crystals suitable for single-crystal X-ray diffraction (SCXRD) were typically obtained by slow solvent evaporation from solution. Carvacrol was purchased from Frey+Lau GmbH and used as such. All of the other reagents and solvents were purchased from Sigma-Aldrich Chemical Co. and used as such.

1 was prepared by manually grinding 1 mmol of INA (122 mg) and 1 mmol of THY (150 mg) in an agate mortar. The solid−solid reaction occurred in 20 min, and a whitish powder was obtained. Single crystals of **1** were obtained after 1 month by slow evaporation of a 1:1 mixture of ethanol and acetone containing INA and THY in equimolar amounts.

2 was prepared by directly mixing 1 mmol of INA (122 mg) and 1 mmol of CAR (154 μL) in an agate mortar. The liquid−solid reaction occurred after 30 min of grinding, and a whitish powder was obtained. After testing several solvents with different polarities, single crystals of **2** were obtained after 1 month by slow evaporation of DMF solution containing equimolar amounts of INA and CAR.

3 was prepared by manually grinding 1 mmol of PYR (80 mg) and 2 mmol of THY (300 mg) in an agate mortar for 10 min, resulting in a homogeneous solid-phase mixture. Single crystals of **3** were obtained after 1 month by slow evaporation of an acetone solution containing PYR and THY in a 1:2 stoichiometric ratio.

4 was prepared by directly mixing 1 mmol of PYR (80 mg) and 4 mmol of CAR (616 μL) in an agate mortar and manually grinding for 10 min, resulting in a viscous paste. Single crystals of **4** were obtained after

https://doi.org/10.1021/acssuschemeng.2c01257
ACS Sustainable Chem. Eng. 2022, 10, 8388−8399

1 month by slow maturation of the viscous paste in a closed vial at ambient conditions.

5a was prepared by manually grinding 1 mmol of TMP (136 mg) and 1 mmol of THY (150 mg) in an agate mortar for 10 min, resulting in a homogeneous solid-phase mixture. Single crystals of **5a** were obtained after 1 month by slow evaporation of a tetrahydrofuran (THF) solution containing TMP and THY in equimolar amounts.

5b was first obtained from the conversion of **5a** after 2 weeks at ambient conditions. It was then resynthesized by ball milling 1 mmol of TMP (136 mg) and 2 mmol of THY (150 mg) with the same protocol described above. Single crystals of **5b** were directly found in the sample container after conversion from **5a**.

6 was prepared by directly mixing 1 mmol of TMP (136 mg) and 2 mmol of CAR (308 μL) in an agate mortar and manually grinding for 10 min, resulting in a homogeneous solid-phase mixture. Single crystals of **6** were obtained after a week by slow evaporation of a diethyl ether solution containing TMP and CAR in a 1:2 stoichiometric ratio.

7 was prepared by manually grinding 1 mmol of DMQ (158 mg) and 1 mmol of THY (150 mg) in an agate mortar and manually grinding for 10 min, resulting in a homogeneous solid-phase mixture. Single crystals of **7** were obtained after 1 month by slow evaporation of a THF solution containing DMQ and THY in equimolar amounts.

8 was prepared by directly mixing1 mmol of DMQ (158 mg) and 2 mmol of CAR (308 μL) in an agate mortar and manually grinding for 10 min, resulting in a homogeneous solid-phase mixture. Single crystals of **8** were obtained after 1 month by slow evaporation of an acetone solution containing DMQ and CAR in a 1:2 stoichiometric ratio.

For each case, the experiment was also repeated with different possible stoichiometric ratios of reactants (determined by the number of acceptor moieties in the coformer). However, except for **5a** and **5b**, these experiments always yielded the reported cocrystal and an excess reactant. Once ascertained that the cocrystals could be formed mechanochemically, all of the samples were resynthesized in bulk with the ball milling method to minimize the presence of unreacted reagents. A Retsch PM100 planetary ball mill equipped with stainless steel 12 mL grinding jars and 10 mm diameter balls was used. The samples were ground for 30 min at 500 rpm speed, inverting the rotation direction at half-time. In the case of **4** and **8**, the heat generated during the milling prevented the cocrystal formation due to their low melting point, and the samples were obtained by freezing the liquid mixture using liquid nitrogen.

Powder X-ray Diffraction (PXRD). The purity and the stoichiometry ratio for all of the samples were checked by PXRD. The data were collected on a Rigaku Smartlab XE diffractometer in $\theta-\theta$ Bragg–Brentano geometry with Cu Kα radiation. The samples were placed on glass supports and exposed to radiation ($1.5° \leq 2\theta \leq 50°$) at a scan rate of 10 °/min. The diffracted beam was collected on a two-dimensional (2D) Hypix 3000 solid-state detector; 5° radiant Soller slits were used as a compromise for high flux and moderate peak asymmetry at low angles. A beam stopper and antiscatterer air component were used to mitigate the scattering at a low angle. All of the experimental data were refined with a Pawley fit against the cell parameters extracted from SCXRD analyses opportunely refined to compensate for the difference in the data collection temperature (see Figures S1–S9).

Time-Resolved In Situ PXRD Monitoring. Time-resolved in situ powder X-ray diffraction (TRIS-PXRD) measurements of the **5a** → **5b** conversion were carried out in parallel beam geometry with Cu Kα radiation on a Rigaku Smartlab XE diffractometer equipped with an Anton-Paar TTK600 nonambient chamber with a flat copper sample holder. The Hypix 3000 solid-state detector was used in 2D mode with an acquisition time of 3 s. Data collection was performed in vacuum at 45 °C to speed up the conversion process, acquiring 2D images at 1 min intervals for 50 min. Powder patterns were extrapolated integrating the resulting 2D images in the range of $175° < \beta > 185°$ to obtain a 2θ range of 5–19°. Results are reported in Figure S29.

Single-Crystal X-ray Diffraction. The diffracted intensities of selected single crystals of **1**–**3**, **5a**, **5b**, and **6**–**7** were collected under nitrogen flux at 180 K on a SMART APEX2 diffractometer using Mo Kα radiation (λ = 0.71073 Å). Data collection for **8** was instead performed under nitrogen flux at 220 K on a Bruker D8 Venture diffractometer using micro-focused Cu Kα radiation (λ = 1.54178 Å), equipped with a kappa goniometer and an Oxford Cryostream. Lorentz polarization and absorption corrections were applied for all of the experiments. Data reduction was carried out using APEX v3 software. Data for **4** were collected with synchrotron radiation under nitrogen flux at 100 K at the XRD1 beamline of Elettra (Trieste, Italy), employing a NdBFe Multipole Wiggler (Hybrid linear) insertion device. The energy of the beam was set to obtain a wavelength of 0.700 Å. The beam size full width at half-maximum (FWHM) was 2.0 × 0.37 mm^2 (0.7 × 0.2 mm^2 FWHM beam size on the sample) with a photon flux of 1012–1013 ph/s. The diffracted intensities were collected on a Pilatus 2M detector and processed using XDS software. All of the structures were solved by direct methods using SHELXT[63] and refined by full-matrix least-squares on all F^2 using SHELXL[64] as implemented in Olex2,[65] using anisotropic thermal displacement parameters for all nonhydrogen atoms (see Figures S10–S18 for ORTEP diagrams). Table S1 reports crystal data collection parameters and refinement results.

Thermal Analysis. Differential scanning calorimetry (DSC) analysis of cocrystal samples (Figures S19–S26) was performed with a PerkinElmer Diamond equipped with a model ULSP 90 ultracooler. Heating was carried out in closed 50 μL Al-pans at 5 °C/min in a variable temperature range, with two heating ramps and a cooling one. Measurements were performed at atmospheric pressure under a constant flow of nitrogen (20 μL/min). The enthalpy of the endothermic or exothermic events was determined by the integration of the area under the DSC peak (see Table S11). Once the peak representing the melting of the cocrystal was identified, melting temperature (T_m) intervals were obtained by averaging, respectively, the onset temperatures and the peak maximum temperatures of the two heating ramps.

Thermogravimetric analysis (TGA) was performed with a PerkinElmer TGA 8000 instrument (mass sample: 1–3 mg), under nitrogen flux (30 mL/min) in the temperature range of 25–120 °C, at 5 °C/min (Figures S27 and S28).

Headspace–Gas Chromatography–Mass Spectrometry (HS–GC–MS) Analysis. One milligram of THY and CAR (1.01 ± 0.04 mg, n = 24) and the corresponding amount of each cocrystal sample (calculated taking into consideration the stoichiometric ratio) were introduced into 10 mL glass vials and maintained uncapped under a laminar flow hood at room temperature (25.2 ± 0.5 °C; n = 3 measurements per day; N = 24 days) for 1 h, 3, 7, and 14 days, respectively. Then, vials were sealed with poly(tetrafluoroethylene) (PTFE)/silicone septa and submitted to HS–GC–MS analysis. Three independent replicated measurements were performed.

One milliliter of the headspace above the sample was introduced into the gas chromatograph injection port by means of a PAL COMBI-xt autosampler (CTC Analytics AG, Zwingen, Switzerland). Before the injection, each sample was equilibrated at 30 °C for 5 min.

Analyses were carried out by means of an HP 6890 Series Plus gas chromatograph equipped with an MSD 5973 mass spectrometer (Agilent Technologies, Milan, Italy). An Rxi-5Sil MS capillary column (30 m length × 0.25 mm i.d., 0.25 μm film thickness; Restek, Bellafonte) and the following temperature program were used for the chromatographic separation: 70 °C, held for 0.50 min, 15 °C/min to 220 °C, held for 1.50 min (runtime: 12.00 min). The analyses were carried out at the constant flow rate of 1.3 mL/min using helium as the carrier gas. The split/splitless injector was held at 270 °C and the injection was executed in split mode (split ratio: 10:1) using a 5183–4647 liner (Agilent Technologies). The transfer line was maintained at 280 °C. The electron ionization–single quadrupole mass spectrometer (EI–MS; 70 eV) was operated in full-scan mode in the 40–200 m/z mass range (scan rate: 4.45 scans/s; electron multiplier voltage: 2.718 kV). The ion source and quadrupole temperatures were set at 230 and 150 °C, respectively. A solvent delay of 2.00 min was applied. Chromatographic data were recorded using the HP ChemStation (Agilent Technologies) software.

Statistical Analysis. After signal normalization through the response factors, one-way analysis of variance (ANOVA) was carried

https://doi.org/10.1021/acssuschemeng.2c01257
ACS Sustainable Chem. Eng. 2022, 10, 8388–8399

out to highlight statistically significant differences across the timescale (α = 0.05). For statistically significant results, the effect size was estimated in terms of Cohen's η^2,[66] and the normalized responses were compared timewise by carrying out unpaired Student's *t*-tests by applying a Bonferroni correction (overall α = 0.05). Normality and homoscedasticity assumptions were verified by means of Shapiro-Wilk's test and Bartlett's test, respectively (both α = 0.05).

Analysis of Stability vs Time under Ambient Conditions. Twenty milligrams (21.30 ± 2.98 mg; n = 33) of all cocrystal samples and pure THY and CAR were introduced into 10 mL glass vials and maintained uncapped under a laminar flow hood at room temperature (27.0 ± 0.4 °C; n = 3 measurements per day; N = 11 days). Each vial was periodically weighted to monitor the mass loss over a period of 14 days. Each test was independently replicated n = 3 times. An additional vial for each sample was treated under the same experimental conditions and used to simultaneously collect PXRD data after 1, 3, 7, 11, and 15 days.

Theoretical Calculations. Intermolecular interaction energies (IIEs) for the first coordination sphere in all cocrystals and pure **THY** structures were calculated using CrystalExplorer17 software package[67] at the CE-B3LYP/6-31G(d,p) level. Energy frameworks[68,69] for a sphere of 3.80 Å around the formula unit are reported in Figures S40−S49.

Periodic DFT calculations were performed with the software CRYSTAL14[70] using the hybrid functional B3LYP. The experimental XRD cocrystal structures were used as a starting guess for geometry optimizations. Basis sets for C (6-31d1G),[71] N (6-31d1G),[71] O (6-31d1G),[71] and H (3−1p1G)[71] atoms were obtained from the CRYSTAL library. London-type pairwise empirical correction to the energy was used to account for dispersion effects.[72] Results of the calculations and optimized structures are reported in Tables S15−S22 and Figures S51−S58.

RESULTS AND DISCUSSION

Crystal Structures. **1** (INA−THY; T_m = 67−69 °C) crystallizes in the *P*21/*c* space group with a 1:1 molar ratio and one formula unit in the asymmetric unit. Two molecules of INA interact via a classical dimeric head-to-head hydrogen-bonding motif between the amidic groups (N···O distance 2.884(2) Å). On the other end of each INA molecule, the pyridinic nitrogen forms an HB with the hydroxyl group of a molecule of THY (O···N distance 2.739(3) Å).

This assembly creates a hydrogen-bonded chain of four molecules, with the INA···INA dimer sandwiched by THY molecules in terminal position (THY···INA···INA···THY), as shown in Figure 2a. The head-to-head dimeric arrangement is a rather strong synthon (see Cambridge Structural Database (CSD) statistics in Figures S59 and S60) and results to be the most stabilizing for the crystal packing, with an IIE of −62.1 kJ/mol, calculated with CrystalExplorer17 at the CE-B3LYP//6-31G(d,p) level. This motif is also present in polymorph I of INA crystal structure,[73] where it presents a similar IIE (−61.9/−63.3 kJ/mol). The IIE of the molecular pair containing the HB between the hydroxyl group of THY and the pyridinic nitrogen of INA is estimated at −39.5 kJ/mol. Another important stabilizing interaction is the one between the amidic group of INA and the aromatic ring of THY, which connects two slabs of tetramers and has an energy of −30.4 kJ/mol (Figure S40).

2 (INA−CAR; T_m = 63−65 °C) also crystallizes in the *P*21/*c* space group with a 1:1 stoichiometric ratio and one formula unit in the asymmetric unit. The main motifs observed in **1**, i.e., the homomeric head-to-head hydrogen-bonding motif between the amidic groups (N···O distance 2.948(2) Å) and the heteromeric hydroxyl-pyridine hydrogen-bond (O···N distance 2.757(2) Å), are also observable in the crystal structure of **2**, leading to the formation of a CAR···INA···INA···CAR tetramer. In this structure, however, the hydroxyl oxygen atom also functions as an HB acceptor and affords an extra interaction with an N−H moiety of the amide group of INA (N···O distance 3.265(3) Å) on both sides of the tetramer (see Figure 2b). Since the CAR molecules accepting the HB are themselves part of other tetramers (with angles between the tetramers mean planes of ca. 80°), a sort of zig-zag ladder between tetramers is generated (see Figure S41). Expectedly, the IIEs for molecular pairs containing the amide−amide head-to-head and the hydroxyl-pyridine motifs, respectively −57.1 and −40.1 kJ/mol, are comparable to those reported for **1**. The energy value of the N−H···O interaction linking the tetramers, in accordance with its longer HB distance, is assessed at just −24.8 kJ/mol.

3 (PYR−THY; T_m = 46−50 °C) crystallizes in the *P*21/*c* space group with a 1:2 stoichiometric ratio and one formula unit (three independent molecules) in the asymmetric unit. Each atom of the PYR molecule is facing a different THY molecule, creating a hexagon of THY molecules surrounding the PYR one (see Figure S42). This geometric assembly hampers the formation of the $\pi\cdots\pi$ stacking interaction characteristic of all PYR polymorphs. PYR nitrogen atoms are involved in HBs with the hydroxyl groups of the THY molecules facing them (O···N distances of 2.798(2) and 2.803(2) Å; Figure 3a). Two PYR hydrogen atoms are involved in C−H···π interactions with the aromatic rings of the THY molecules facing them (Figure 3a). The remaining two hydrogen atoms of PYR face other two THY molecules that do not seem to be interacting with PYR but display approximate edge-to-face interactions with the neighbor-

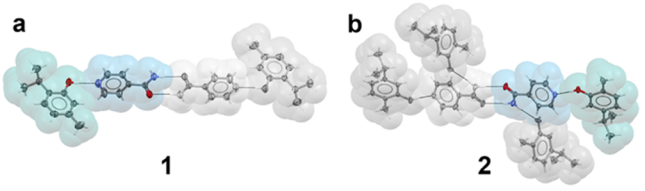

Figure 2. Molecular assembly in cocrystals **1** (INA−THY 1:1) (a) and **2** (INA−CAR 1:1) (b). C, N, and O atoms are represented, respectively, by gray, blue, and red ellipsoids, while H atoms are reported as white capped sticks. Each molecule is superimposed to its van der Waals surface with arbitrary colors based on symmetry equivalence. Molecules outside of the formula unit are grayed out. Black dotted lines represent selected interactions.

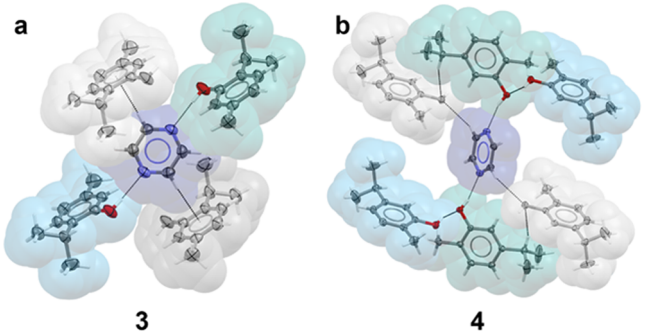

Figure 3. Molecular assembly in cocrystals **3** (PYR−THY 1:2) (a) and **4** (PYR−CAR 1:4) (b). C, N, and O atoms are represented, respectively, by gray, blue, and red ellipsoids, while H atoms are reported as white capped sticks. Each molecule is superimposed to its van der Waals surface with arbitrary colors based on symmetry equivalence. Molecules outside of the formula unit are grayed out. Black dotted lines represent selected interactions.

https://doi.org/10.1021/acssuschemeng.2c01257
ACS Sustainable Chem. Eng. 2022, 10, 8388−8399

ing THY molecules in the hexagon (those involved in the O−H···N HBs). Energy framework calculations show that the packing is dominated by coulombic forces, mostly due to the stabilizing contribution of the HBs between THY and PYR (total energy values of −35.5 and −36.2 kJ/mol). Mostly of a dispersive nature are instead the above-mentioned edge-to-face interaction between THY molecules (−22.1 and −22.7 kJ/mol, see Figure S42), and the C−H···π interactions between PYR and THY (−17.7 and −17.8 kJ/mol).

4 (PYR−CAR; T_m = 17−21 °C) crystallizes in the $C2/c$ space group with a 1:4 stoichiometric ratio. The asymmetric unit is composed of two independent CAR molecules and half a molecule of PYR lying on an inversion center. The two symmetry-independent molecules of CAR are hydrogen-bonded to each other (O···O distance 2.753(1) Å) and one of them is also hydrogen-bonded to the N atom of PYR (O···N distance 2.761(1) Å). This arrangement forms a motif in which trimeric units analogous to those of **3** can be observed, with additional terminal CAR···CAR HBs as displayed in Figure 3b. As expected, the most stabilizing energetic contributions to the crystal packing are those of the two HBs, with −34.1 and −29.4 kJ/mol respectively for CAR···PYR O−H···N and for CAR···CAR O−H···O. As for **3**, we can observe dispersive edge-to-face interactions between the EO aromatic rings connecting the trimeric units (−20.7 kJ/mol). Moreover, an interaction between CAR molecules exhibiting a contact between the isopropyl and hydroxyl groups accounts for −21.2 kJ/mol (mixed dispersive-coulombic nature).

5a (TMP−THY; T_m = 61−63 °C) crystallizes in the $P\bar{1}$ space group with a 1:1 stoichiometric ratio, two formula units, and four independent molecules in the asymmetric unit. Each of the two independent molecules of TMP is H-bonded to an independent molecule of THY (O···N distances 2.787(2) and 2.769(2) Å), assembling in two symmetry-independent PYR···THY dimers. These dimers are connected via $\pi\cdots\pi$ interactions between the two PYR molecules. One of the two pyrazines also forms a parallel $\pi\cdots\pi$ interaction with its symmetry equivalent counterpart from another dimer, while in the other direction the presence of a THY molecule hampers the formation of an infinite columnar stacking. As visible in Figure 4a, we have

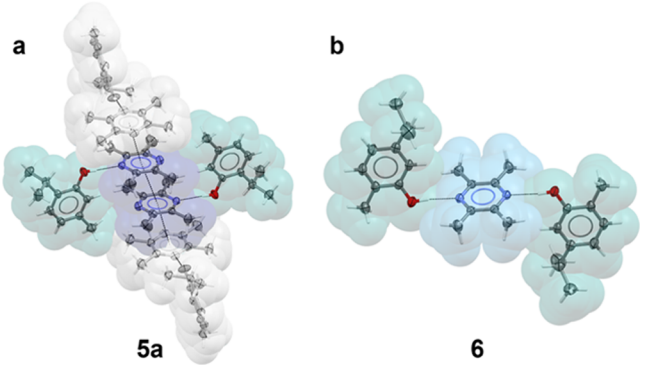

Figure 4. Molecular assembly in cocrystals **5a** (TMP−THY 1:1) (a) and **6** (TMP−CAR 1:2) (b). C, N, and O atoms are represented, respectively, by gray, blue, and red ellipsoids, while H atoms are reported as white capped sticks. Each molecule is superimposed to its van der Waals surface with arbitrary colors based on symmetry equivalence. Molecules outside of the formula unit (or asymmetric unit in the case of **5a**) are grayed out. Black dotted lines represent selected interactions.

therefore a stacking of four PYR molecules sandwiched by THY molecules, with contacts on the isopropyl side. The terminal $\pi\cdots\pi$ interactions have a distance of 3.602 Å between ring centroids and an angle of 6.15° between the ring mean planes, while the inner interaction has a distance of 3.889 Å and an angle of 0°. For the central interaction, the molecules of PYR are stacked on top of each other with the same orientation, while the terminal ones display a staggered orientation that reduces repulsion between methyl groups, and adds a coulombic stabilization effect to the mostly dispersive interaction energy (resulting in a total IIE of −40.3 vs the −24.7 kJ/mol of the central interaction).[42] Several other dispersive interactions between THY molecules contribute to stabilizing the crystal packing, but the strongest interactions are the HBs between TMP and THY molecules, with IIEs of −47.0 and −49.9 kJ/mol.

6 (TMP−CAR; T_m = 58−60 °C) crystallizes in the $P21/c$ space group with a 1:2 stoichiometric ratio. The asymmetric unit is composed of a molecule of CAR and half a molecule of TMP lying on an inversion center. As shown in Figure 4b, the molecule of TMP is engaged in two HBs with symmetry equivalent molecules of CAR (O···N distance 2.831(2) Å; IIE −48.1 kJ/mol). The rest of the crystal packing is governed by many weak steric interactions, which connect the HB containing trimeric units to form pillars along the crystallographic b axis. The most stabilizing of such interactions is the one responsible for the formation of the pillars and has an energy value of −21.0 kJ/mol (isopropyl···ring contact between two molecules of CAR along the b axis).

7 (DMQ−THY; T_m = 71−74 °C) crystallizes in the $P21/n$ space group with a 1:1 stoichiometric ratio and one formula unit in the asymmetric unit. DMQ interacts with THY through an HB (O···N distance 2.781(2) Å) accounting for −46.1 kJ/mol. The DMQ···THY dimers are arranged in pillars via $\pi\cdots\pi$ interactions between DMQ molecules. The parallel stacking, as shown in Figure 5a, is formed of two alternating interactions. In

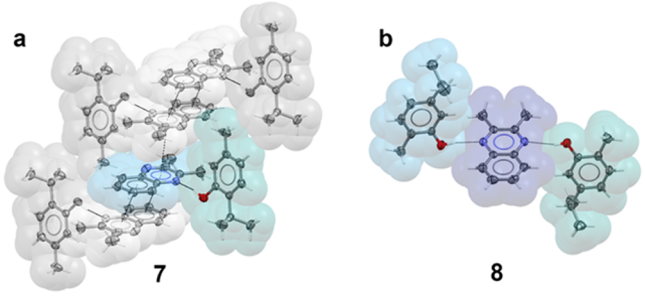

Figure 5. Molecular assembly in cocrystals **7** (DMQ−THY 1:1) (a) and **8** (DMQ−CAR 1:2) (b). C, N, and O atoms are represented respectively by gray, blue, and red ellipsoids, while H atoms are reported as white capped sticks. Each molecule is superimposed to its van der Waals surface with arbitrary colors based on symmetry equivalence. Molecules outside of the formula unit are grayed out. Black dotted lines represent selected interactions.

the first, accounting for −28.0 kJ/mol, the DMQ molecules are oriented in opposite ways, with the substituted heteroaromatic ring facing the unsubstituted ring and *vice versa* (distance of 3.826 Å between each couple of ring centroids). In the second and more stabilizing interaction, accounting for −31.1 kJ/mol, the molecules are also oriented in alternate ways, but they display a greater offset, in a way that only the two alternating substituted heteroaromatic rings are directly on top of each

https://doi.org/10.1021/acssuschemeng.2c01257
ACS Sustainable Chem. Eng. 2022, 10, 8388−8399

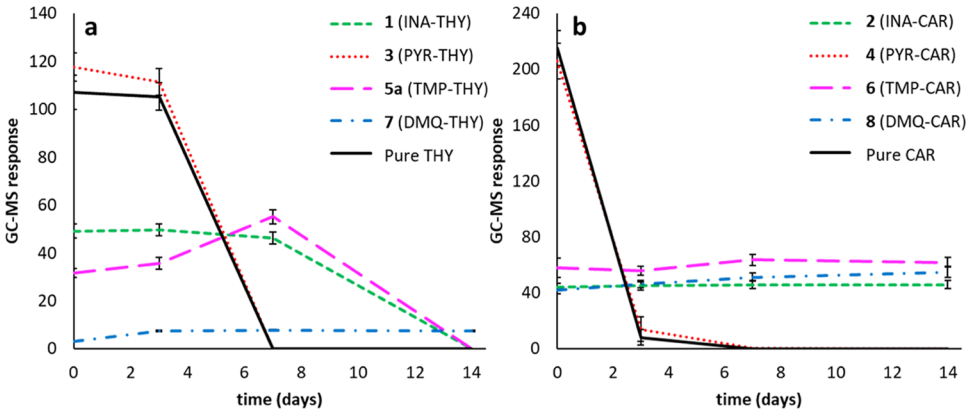

Figure 6. Release profile of the active components of the essential oils at room temperature from thymol-based (namely, **1**, **3**, **5a**, and **7**) (a) and carvacrol-based cocrystals (namely, **2**, **4**, **6**, and **8**) (b). Release profiles of pure THY (a) and CAR (b) are also reported for comparison. Responses are normalized using the proper response factor (n = 3).

other (ring centroids distance of 3.893 Å). The rest of the crystal packing is composed of weaker steric interactions.

8 (DMQ−CAR; T_m = 30−34 °C) crystallizes in the $P2_1$ space group with a 1:2 stoichiometric ratio and one formula unit in the asymmetric unit. In contrast to that observed for **7**, both nitrogen atoms of DMQ are here involved in HBs with two symmetry-independent molecules of CAR (O···N distances 2.888(4) and 2.920(4) Å; IIEs of −30.6 and −30.4 kJ/mol respectively). The so-formed trimeric units (Figure 5b) are arranged in pillars along the crystallographic axis b, related to the neighboring pillar along a by a twofold axis, and to those along c by an inversion center. Moreover, the trimeric units are interconnected by weak dispersive interactions between the methyl group of CAR and the phenyl ring of the DMQ with the isopropyl and methyl moieties of two adjacent CAR molecules.

Release of EO Active Components from Cocrystals. All of the cocrystals, THY, and CAR were analyzed *via* HS−GC−MS to investigate the release of the EO active components over a period of 14 days at room temperature. The normalized release profiles are reported in Figure 6. A full breakdown of the data and the results of time-to-time ANOVA are reported in Tables S12 and S13.

In most of the cases, cocrystallization affects both the short- and long-term release of the EO active components. A noticeable decrease in acute delivery is compensated by a prolonged release compared to the pure components, which in some instances persists along 14 days.

In the case of cocrystals **3** and **4** containing PYR (Figure 6, red dotted lines), the release profiles mimic almost exactly the behavior of pure THY and CAR, respectively (Figure 6, black solid lines). These findings were not surprising for cocrystal **4**, as due to its low melting point, it tends to liquefy at room temperature decomposing into the coformers, but they were unexpected for **3**. The release profiles for the rest of the cocrystals containing CAR (Figure 6b) are similar to each other and in line with expectations; in all three cases we observe a decrease of up to 27 standard deviations[74] in the acute response with respect to pure carvacrol and a stabilized release (p > 0.05; Bonferroni adjusted) that spans the entire investigated time window (14 days). The same applies for sample **7** containing THY (DMQ−THY; Figure 6a, blue dot-dashed line), although the observed GC−MS response is considerably lower (6−36 standard deviations)[74] than for its CAR containing analogue **8** (DMQ−CAR; Figure 6b, blue dot-dashed line). For sample **1** (INA−THY; Figure 6a, green dashed line) we also observe a stabilized release during the first 7 days (p > 0.05; Bonferroni adjusted), but no GC−MS response was detected on the 14th day. Finally, the most peculiar case is presented by sample **5a** (TMP−THY; Figure 6a, magenta long-dashed line). As in the case of **1**, no response was detected on the 14th day, but the profile became steeper between the third and seventh days, highlighting an interesting increase (p < 0.05; Bonferroni adjusted) of THY release after the acute response. Summing up, the release of THY and CAR in cocrystals over 14 days is generally more persistent than that of the pure substance, indicating the possibility of exploiting cocrystallization to tune the EO components' environmental emission. The release profiles of certain samples, however, presented unexpected features or peculiarities that we addressed and explained with additional investigations on their stability.

Stabilization Energy (SE) of EO Active Components. A rationalization of the results was attempted on the basis of the periodic DFT energies calculated with CRYSTAL14,[70] normalized to the number of THY or CAR molecules in the unit cell (Table S15 and Figure S50). This energy value (SE) should correspond to the stabilization of the active component in each cocrystal structure. The SEs trend for the CAR-based cocrystals qualitatively correlates with the release profiles. **4** is individuated as the least stable and the stability order of **2**, **8**, and **6** corresponds to the order observed in the prolonged release. In the case of THY-based cocrystals, it is more difficult to compare the prolonged releases because of the peculiarities described above, but **3** and **7** are correctly individuated as the least and most stable respectively, and the order of **1** and **5a** corresponds to the one observed for the acute release. Of course, this computational assessment of relative stabilities between the different cocrystals does not consider several variables that could have affected the HS−GC−MS experiment, such as granulometry of the samples and temperature.

Analysis of Stability vs Time under Ambient Conditions. To explore the behavior of the eight cocrystals under conditions similar to those of the HS−GC−MS experiment and to shed more light on the reasons behind the peculiarities of the release profiles, a stability test at ambient conditions was carried out as described in the Experimental Section. The mass loss trends over 14 days (Figure S30) follow the same order for THY- and CAR-based cocrystals, although the THY-based ones generally display slightly higher values. In both cases, the least

https://doi.org/10.1021/acssuschemeng.2c01257
ACS Sustainable Chem. Eng. 2022, 10, 8388−8399

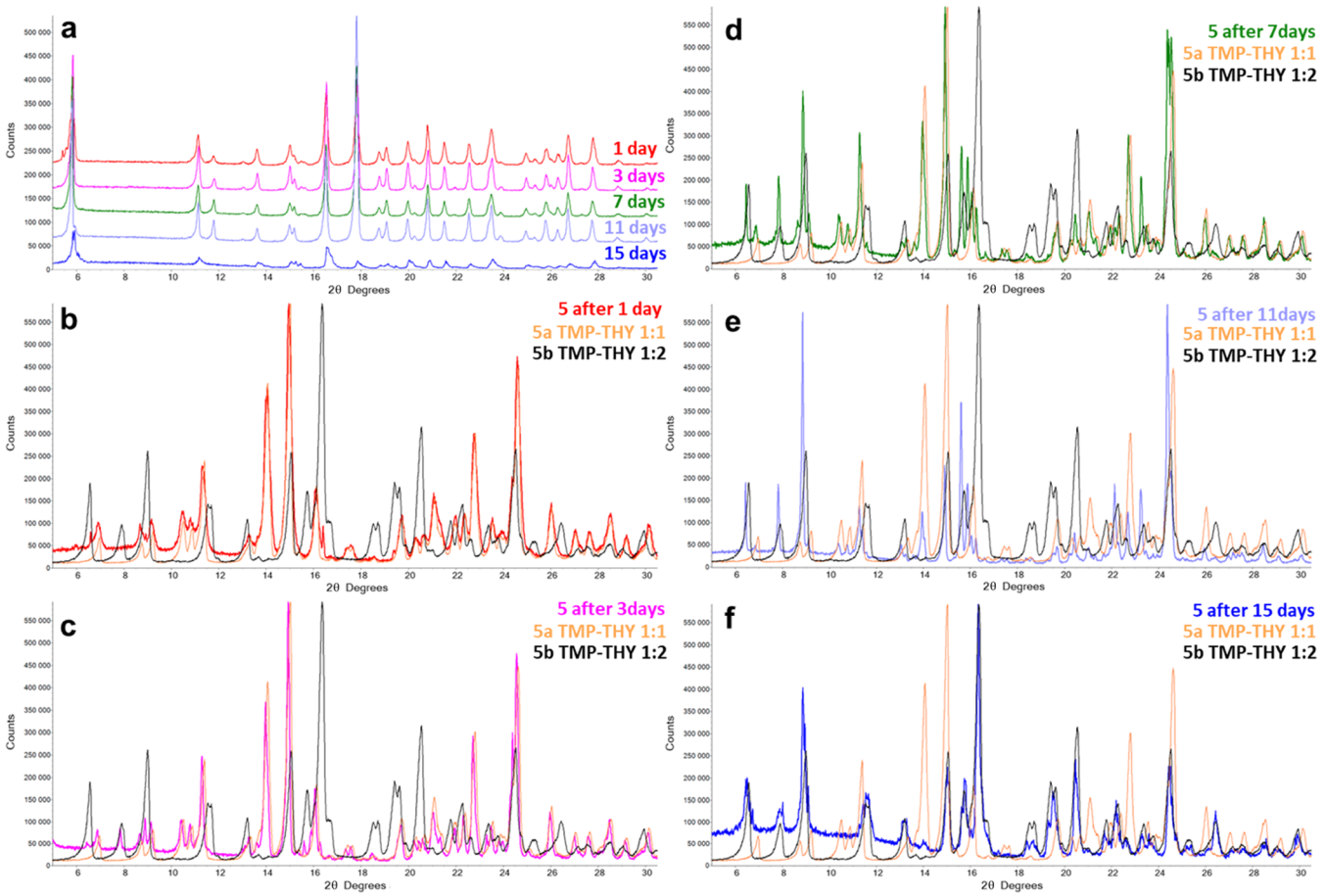

Figure 7. (a) Evolution of the powder pattern of sample **5** in the span of 15 days. (b) Comparison of the powder pattern after 1 day (red) with the initial patterns of **5a** (orange) and **5b** (black). (c) Comparison of the powder pattern after 3 days (magenta) with the initial patterns of **5a** (orange) and **5b** (black). (d) Comparison of the powder pattern after 7 days (green) with the initial patterns of **5a** (orange) and **5b** (black). (e) Comparison of the powder pattern after 11 days (indigo) with the initial patterns of **5a** (orange) and **5b** (black). (f) Comparison of the powder pattern after 15 days (blue) with the initial patterns of **5a** (orange) and **5b** (black).

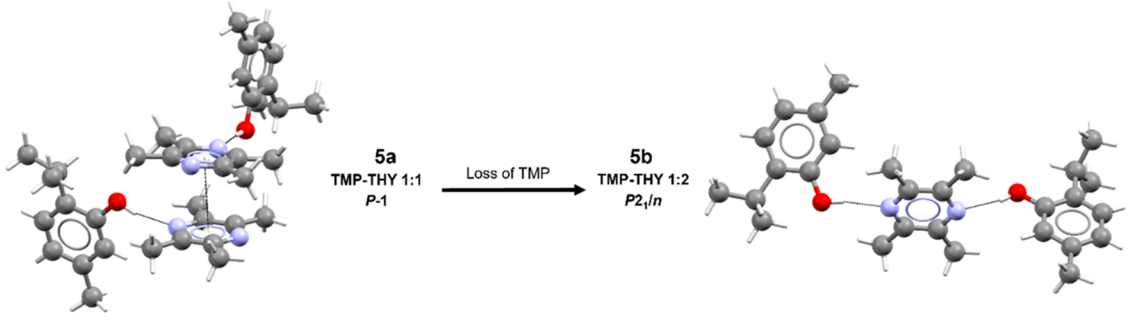

Figure 8. Scheme of the conversion from **5a** (TMP−THY 1:1) to **5b** (TMP−THY 1:2). C, N, and O atoms are represented, respectively, by gray, blue, and red spheres, while H atoms are reported as white capped sticks. Black dotted lines represent selected interactions.

mass loss is observed for DMQ-based cocrystals **7** and **8**, followed by INA-based **1** and **2**, and TMP-based **5a** and **6**. Cocrystals with PYR as coformers **3** and **4** exhibit a greater mass loss than the pure components themselves, indicating once again their instability and their components' tendency to sublimate or evaporate.

Figures 7 and S31−S39 show the powder patterns collected at different time steps of the experiment for the different samples. In the case of **3**, decomposition of the cocrystal was observed (Figure S33). Already after 1 day (Figure S34), the process is well underway, and after 3 days (Figure S35), the pattern of the sample is completely superimposable to the pattern of pure THY (due to sublimation of PYR). No patterns are available for sample **4** because it decomposed and liquefied after a few minutes from the start of the experiment. These observations suggest an intrinsic instability of the PYR containing cocrystals **3** and **4**, in agreement with their release profiles (almost identical to those of the pure EOs components) and the periodic DFT calculated SEs.

Sample **5a**, on the other hand, transformed to a new phase **5b** after 15 days (Figure 7f). SCXRD analysis of the new phase showed that **5a** (TMP−THY 1:1) underwent loss of TMP and

https://doi.org/10.1021/acssuschemeng.2c01257
ACS Sustainable Chem. Eng. 2022, 10, 8388−8399

converted to a new cocrystal form with different stoichiometry **5b** (TMP−THY 1:2; Figure 8). The **5a**-to-**5b** conversion is likely to be the cause for the peculiarities in **5a** release profile. Indeed, as evident from Figure 7, peaks of **5b** already start to appear after the third day (Figure 7c) and increase with time (Figure 7d,e) until the sample is completely converted at the end of the experiment (Figure 7f). The time frame, therefore, coincides quite well with the increase of THY release in the HS−GC−MS profile of **5a**. We monitored the same experiment starting from freshly synthesized **5b** (resynthesized in pure form by ball milling) and no variation in its PXRD has been observed within a 15-day period (Figure S39).

5a-to-5b Conversion. The structure of **5b** (TMP−THY 1:2) crystallizes in the $P21/n$ space group and presents similar motifs to those of its CAR analogue **6** (TMP−CAR 1:2). We can speculate that the driving force of the **5a**-to-**5b** conversion is related to the fact that both of the pyridinic nitrogen atoms in TMP act as the HB acceptor in **5b**, thus causing the change of the coformers stoichiometry. However, a statistical analysis performed interrogating the CSD by CCDC[75] reveals that there is no marked prevalence of 1:2 over 1:1 stoichiometries for the pyrazine-derived coformers as those employed in this work (Figure S61). Indeed, in the case of PYR, we have a 46% of binary cocrystals adopting a 1:1 stoichiometry and a 45% with a 1:2 ratio. In the case of TMP, the 1:1 stoichiometry is even more common, with a 46% against the 32% of the 1:2 ratio. For DMQ we report a prevalence of the 1:1 ratio, although the number of the observations reported in the CSD is not statistically reliable to allow us to draw any relevant conclusion.

Notably, no Bragg reflections associated with the reagents were ever observed in any PXRD patterns over the conversion process (Figure 7). This observation might bring us to conclude that **5a** is a metastable phase. The crystal structure dissociation is followed by the coformers' sublimation. The remaining parts recombine into a more stable cocrystal structure with a different stoichiometric ratio. Interestingly, **5a** has two formula units in the asymmetric units, and $Z' > 1$ crystals have been speculated to often be kinetic metastable products.[76−80]

Fortuitously, the relation between the **5a**-to-**5b** transformation and the increase of THY release in the HS−GC−MS profile could be a quite appealing feature for applications as a "smart" material for active packaging. A delayed boost of the active component release, indeed, would be ideal if it were to coincide with the time window after which the food spoilage bacteria growth starts becoming more significant. Discovering a plethora of materials for which this phenomenon occurs in different time windows would allow one to tune the active component release depending on the desired food to preserve. High Z' cocrystals of EOs components could be a good starting point to further investigate this application in the future.

CONCLUSIONS

The exploitation of EOs in the fields of agriculture and food preservation is often hampered by their physical properties. Cocrystallization can serve as a way to tune such properties and extend their range of applicability, making it easier to use them as an alternative to conventional pesticides or synthetic food additives. Here we presented a series of cocrystals based on THY and CAR with four different coformers. All of these materials were successfully obtained with sustainable and cost-effective mechanochemical procedures and were fully and thoroughly characterized.

The analysis of their release profiles highlighted that cocrystallization was successful in modulating the environmental release of the active components, decreasing their acute response, and stabilizing it over time. This is especially true for cocrystals based on the liquid component CAR, which showed a persistent release for at least 14 days at room temperature.

However, PYR proved not to be a suitable coformer for stabilizing THY and CAR in a more stable co-crystalline form. Indeed, PYR−THY and PYR−CAR cocrystals showed a tendency to quickly decompose in the original components.

Finally, the observed conversion from TMP−THY 1:1 to TMP−THY 1:2, accompanied by an increase in the release of the active component, opens attractive possibilities for the development of smart materials for active packaging, capable of releasing more of the active component when the food spoiling process begins. Of course, this particular application should be investigated more in detail, and future efforts will be directed to search for other cocrystals displaying such stoichiometric conversions, hopefully affording a precise tuning of the EO release/time parameter for active packaging applications.

ASSOCIATED CONTENT

Supporting Information

The Supporting Information is available free of charge at https://pubs.acs.org/doi/10.1021/acssuschemeng.2c01257.

Crystallographic data and ORTEP visualization as well as the X-ray powder diffraction patterns and Pawley refinements; differential scanning calorimetry and thermogravimetric analysis; HS−GC−MS data of cocrystal samples and pure EO components; time-resolved in situ PXRD monitoring of **5a** → **5b** conversion; time monitoring of the mass loss and PXRD pattern variation of cocrystal samples; energy frameworks calculations; periodic DFT optimized structures and energies; and coformers' CSD statistics (PDF)

All structures (CIF)

Accession Codes

Accession Codes CCDC 2014877 and 2151107−2151114 contain the supplementary crystallographic data for this paper. These data can be obtained free of charge via www.ccdc.cam.ac.uk/data_request/cif, by emailing data_request@ccdc.cam.ac.uk, or by contacting The Cambridge Crystallographic Data Centre, 12 Union Road, Cambridge CB2 1EZ, UK; fax: +44 1223 336033.

AUTHOR INFORMATION

Corresponding Authors

Paolo P. Mazzeo − *Department of Chemistry, Life Sciences and Environmental Sustainability, University of Parma, 43124 Parma, Italy; Biopharmanet-TEC, University of Parma, 43124 Parma, Italy;* orcid.org/0000-0002-5787-3609; Email: paolopio.mazzeo@unipr.it

Alessia Bacchi − *Department of Chemistry, Life Sciences and Environmental Sustainability, University of Parma, 43124 Parma, Italy; Biopharmanet-TEC, University of Parma, 43124 Parma, Italy;* orcid.org/0000-0001-5675-9372; Email: alessia.bacchi@unipr.it

Authors

Fabio Montisci − *Department of Chemistry, Life Sciences and Environmental Sustainability, University of Parma, 43124 Parma, Italy;* Present Address: Cambridge Crystallographic

https://doi.org/10.1021/acssuschemeng.2c01257
ACS Sustainable Chem. Eng. 2022, 10, 8388−8399

Data Centre, 12 Union Road, Cambridge CB2 1EZ, United Kingdom

Claudia Carraro − *Department of Chemistry, Life Sciences and Environmental Sustainability, University of Parma, 43124 Parma, Italy*

Michele Prencipe − *Department of Chemistry, Life Sciences and Environmental Sustainability, University of Parma, 43124 Parma, Italy*

Paolo Pelagatti − *Department of Chemistry, Life Sciences and Environmental Sustainability, University of Parma, 43124 Parma, Italy; Biopharmanet-TEC, University of Parma, 43124 Parma, Italy;* orcid.org/0000-0002-6926-2928

Fabio Fornari − *Department of Chemistry, Life Sciences and Environmental Sustainability, University of Parma, 43124 Parma, Italy*

Federica Bianchi − *Department of Chemistry, Life Sciences and Environmental Sustainability, University of Parma, 43124 Parma, Italy; Interdepartmental Center for Packaging (CIPACK), University of Parma, 43124 Parma, Italy;* orcid.org/0000-0001-7880-5624

Maria Careri − *Department of Chemistry, Life Sciences and Environmental Sustainability, University of Parma, 43124 Parma, Italy; Interdepartmental Center on Safety, Technologies, and Agri-Food Innovation (SITEIA.PARMA), University of Parma, 43124 Parma, Italy*

Complete contact information is available at: https://pubs.acs.org/10.1021/acssuschemeng.2c01257

Author Contributions

The manuscript was written through contributions of all authors. All authors have given approval to the final version of the manuscript.

Notes

The authors declare no competing financial interest.

■ ACKNOWLEDGMENTS

Chiesi Farmaceutici S.p.A. is acknowledged for the use of the Bruker D8 Venture single-crystal diffractometer. This work was funded by the Ministero delle Politiche Agricole, Alimentari, Forestali e del Turismo (MIPAAFT) by granting for the project PAC/Packaging Attivo Crystallino. This work was promoted by the COMP-HUB initiative, funded by the "Department of Excellence" program of the Italian Ministry for Education, University and Research (MIUR, 2018−2022). This work also benefitted from the 2020 call of the PRIN: Research Projects of Relevant Interest program of the Italian Ministry for University and Research (PRIN2020Y2CZJ2).

■ ABBREVIATIONS

ANOVA, analysis of variance; CAR, carvacrol; DMQ, 2,3-dimethylquinoxaline; DSC, differential scanning calorimetry; EFC, energy framework calculations; GRAS, generally regarded as safe (from FDA or equivalent European regulations); HB, hydrogen bond; HS−GC−MS, headspace−gas chromatography−mass spectrometry; IIE, intermolecular interaction energy; INA, isonicotinamide; PXRD, powder X-ray diffraction; PYR, pyrazine; SCXRD, single-crystal X-ray diffraction; THY, thymol; TMP, 2,3,5,6-tetramethylpyrazine

■ REFERENCES

(1) Isman, M. B. Botanical Insecticides: A Global Perspective. *ACS Symp. Ser.* **2014**, *1172*, 21−30.

(2) Martínez-ballesta, M. C.; López-pérez, L.; Muries, B.; Carvajal, M. Climate Change and Plant Water Balance: The Role of Aquaporins − A Review. In *Climate Change, Intercropping, Pest Control and Beneficial Microorganisms*, Lichtfouse, E., Ed.; Springer: Dordrecht, 2009; pp 71−89.

(3) Singh, N. S.; Sharma, R.; Parween, T.; Patanjali, P. K. Pesticide Contamination and Human Health Risk Factor. In *Modern Age Environmental Problems and their Remediation*, Springer International Publishing: Cham, 2018; pp 49−68.

(4) Gazzurelli, C.; Migliori, A.; Mazzeo, P. P.; Carcelli, M.; Pietarinen, S.; Leonardi, G.; Pandolfi, A.; Rogolino, D.; Pelagatti, P. Making Agriculture More Sustainable: An Environmentally Friendly Approach to the Synthesis of Lignin@Cu Pesticides. *ACS Sustainable Chem. Eng.* **2020**, *8*, 14886−14895.

(5) Gazzurelli, C.; Carcelli, M.; Mazzeo, P. P.; Mucchino, C.; Pandolfi, A.; Migliori, A.; Pietarinen, S.; Leonardi, G.; Rogolino, D.; Pelagatti, P. Exploiting the Reducing Properties of Lignin for the Development of an Effective Lignin@Cu 2 O Pesticide. *Adv. Sustainable Syst.* **2022**, No. 2200108.

(6) Perricone, M.; Arace, E.; Corbo, M. R.; Sinigaglia, M.; Bevilacqua, A. Bioactivity of Essential Oils: A Review on Their Interaction with Food Components. *Front. Microbiol.* **2015**, *6*, No. 76.

(7) Hammer, K. A.; Carson, C. F.; Riley, T. V. Antimicrobial Activity of Essential Oils and Other Plant Extracts. *J. Appl. Microbiol.* **1999**, *86*, 985−990.

(8) Bakkali, F.; Averbeck, S.; Averbeck, D.; Idaomar, M. Biological Effects of Essential Oils - A Review. *Food Chem. Toxicol.* **2008**, *46*, 446−475.

(9) Mossa, A. T. H. Green Pesticides: Essential Oils as Biopesticides in Insect-Pest Management. *J. Environ. Sci. Technol.* **2016**, *9*, 354−378.

(10) Sharma, S.; Barkauskaite, S.; Jaiswal, A. K.; Jaiswal, S. Essential Oils as Additives in Active Food Packaging. *Food Chem.* **2021**, *343*, No. 128403.

(11) Bianchi, F.; Fornari, F.; Riboni, N.; Spadini, C.; Cabassi, C. S.; Iannarelli, M.; Carraro, C.; Mazzeo, P. P.; Bacchi, A.; Orlandini, S.; Furlanetto, S.; Careri, M. Development of Novel Cocrystal-Based Active Food Packaging by a Quality by Design Approach. *Food Chem.* **2021**, *347*, No. 129051.

(12) Conte, A.; Cappelletti, G. M.; Nicoletti, G. M.; Russo, C.; Del Nobile, M. A. Environmental Implications of Food Loss Probability in Packaging Design. *Food Res. Int.* **2015**, *78*, 11−17.

(13) Huang, T.; Qian, Y.; Wei, J.; Zhou, C. Polymeric Antimicrobial Food Packaging and Its Applications. *Polymers* **2019**, *11*, 560.

(14) Kuorwel, K. K.; Cran, M. J.; Sonneveld, K.; Miltz, J.; Bigger, S. W. Essential Oils and Their Principal Constituents as Antimicrobial Agents for Synthetic Packaging Films. *J. Food Sci.* **2011**, *76*, R164−R177.

(15) Ribeiro-Santos, R.; Andrade, M.; Melo, N. R. de.; Sanches-Silva, A. Use of Essential Oils in Active Food Packaging: Recent Advances and Future Trends. *Trends Food Sci. Technol.* **2017**, *61*, 132−140.

(16) Valdés, A.; Ramos, M.; Beltrán, A.; Jiménez, A.; Garrigós, M. State of the Art of Antimicrobial Edible Coatings for Food Packaging Applications. *Coatings* **2017**, *7*, 56−78.

(17) Food and Drug Administration. Rules and Regulations. *Federal Register* **2016**, *81*, 54960−55055.

(18) European Commission. Commission Implementing Regulation (EU) No 872/2012. *Off. J. Eur. Union, L* **2012**, *267*, 1−161.

(19) Csáki, K. F. Synthetic Surfactant Food Additives Can Cause Intestinal Barrier Dysfunction. *Med. Hypotheses* **2011**, *76*, 676−681.

(20) Isman, M. B.; Miresmailli, S. Plant Essential Oils as Repellents and Deterrents to Agricultural Pests. *ACS Symp. Ser.* **2011**, *1090*, 67−77.

(21) Bethanis, K.; Tzamalis, P.; Tsorteki, F.; Kokkinou, A.; Christoforides, E.; Mentzafos, D. Structural Study of the Inclusion Compounds of Thymol, Carvacrol and Eugenol in β-Cyclodextrin by X-Ray Crystallography. *J. Inclusion Phenom. Macrocyclic Chem.* **2013**, *77*, 163−173.

(22) Bacchi, A.; Cantoni, G.; Granelli, M.; Mazza, S.; Pelagatti, P.; Rispoli, G. Hydrogen Bond Optimization via Molecular Design for the Fabrication of Crystalline Organometallic Wheel-and-Axle Com-

pounds Based on Half-Sandwich Ru(II) Units. *Cryst. Growth Des.* **2011**, *11*, 5039−5047.
(23) Bacchi, A.; Cantoni, G.; Pelagatti, P.; Rizzato, S. Dinuclear Arene Ruthenium Dichloro Complexes Designed for Host−Guest Propensity. *J. Organomet. Chem.* **2012**, *714*, 81−87.
(24) Bacchi, A.; Cantoni, G.; Chierotti, M. R.; Girlando, A.; Gobetto, R.; Lapadula, G.; Pelagatti, P.; Sironi, A.; Zecchini, M. Water Vapour Uptake and Extrusion by a Crystalline Metallorganic Solid Based on Half-Sandwich Ru(II) Building-Blocks. *CrystEngComm* **2011**, *13*, 4365−4375.
(25) Balestri, D.; Mazzeo, P. P.; Carraro, C.; Demitri, N.; Pelagatti, P.; Bacchi, A. Stepwise Evolution of Molecular Nanoaggregates Inside the Pores of a Highly Flexible Metal−Organic Framework. *Angew. Chem.* **2019**, *131*, 17503−17511.
(26) Mazzeo, P. P.; Balestri, D.; Bacchi, A.; Pelagatti, P. Stabilization of Liquid Active Guests via Nanoconfinement into a Flexible Microporous Metal−Organic Framework. *CrystEngComm* **2021**, *23*, 7262−7269.
(27) Balestri, D.; Mazzeo, P. P.; Perrone, R.; Fornari, F.; Bianchi, F.; Careri, M.; Bacchi, A.; Pelagatti, P. Deciphering the Supramolecular Organization of Multiple Guests Inside a Microporous MOF to Understand Their Release Profile. *Angew. Chem.* **2021**, *133*, 10282−10290.
(28) Mazzeo, P. P.; Bacchi, A.; Pelagatti, P. Crystal Engineering Guidelines for Ruthenium Based Wheel-and-Axle Compounds. *Coord. Chem. Rev.* **2020**, *414*, No. 213302.
(29) Zigon, N.; Kikuchi, T.; Ariyoshi, J.; Inokuma, Y.; Fujita, M. Structural Elucidation of Trace Amounts of Volatile Compounds Using the Crystalline Sponge Method. *Chem. - Asian J.* **2017**, *12*, 1057−1061.
(30) Gu, X. F.; Zhao, Y.; Li, K.; Su, M. X.; Yan, F.; Li, B.; Du, Y. X.; Di, B. Differentiation of Volatile Aromatic Isomers and Structural Elucidation of Volatile Compounds in Essential Oils by Combination of HPLC Separation and Crystalline Sponge Method. *J. Chromatogr. A* **2016**, *1474*, 130−137.
(31) Zukerman-Schpector, J.; Tiekink, E. R. T. What Is a Co-Crystal? *Z. Kristallogr. - Cryst. Mater.* **2008**, *223*, 233−234.
(32) Aakeröy, C. B.; Salmon, D. J. Building Co-Crystals with Molecular Sense and Supramolecular Sensibility. *CrystEngComm* **2005**, *7*, 439−448.
(33) Zhang, J.; Shreeve, J. M. Time for Pairing: Cocrystals as Advanced Energetic Materials. *CrystEngComm* **2016**, *18*, 6124−6133.
(34) Javoor, M.; Mondal, P.; Chopra, D. Cocrystals: A Review of Recent Trends in Pharmaceutical and Material Science Applications. *Mater. Sci. Res. India* **2017**, *14*, 09−18.
(35) Mazzeo, P. P.; Prencipe, M.; Feiler, T.; Emmerling, F.; Bacchi, A. On the Mechanism of Cocrystal Mechanochemical Reaction via Low Melting Eutectic: A Time-Resolved in Situ Monitoring Investigation. *Cryst. Growth Des.* **2022**, DOI: 10.1021/acs.cgd.2c00262.
(36) Steed, J. W. The Role of Co-Crystals in Pharmaceutical Design. *Trends Pharmacol. Sci.* **2013**, *34*, 185−193.
(37) Almarsson, Ö.; Peterson, M. L.; Zaworotko, M. The A to Z of Pharmaceutical Cocrystals: A Decade of Fast-Moving New Science and Patents. *Pharm. Pat. Anal.* **2012**, *1*, 313−327.
(38) Sandhu, B.; Sinha, A. S.; Desper, J.; Aakeroy, C. B. Modulating the Physical Properties of Solid Forms of Urea Using Co-Crystallization Technology. *Chem. Commun.* **2018**, *54*, 4657−4660.
(39) Mazzei, L.; Broll, V.; Casali, L.; Silva, M.; Braga, D.; Grepioni, F.; Baltrusaitis, J.; Ciurli, S. Multifunctional Urea Cocrystal with Combined Ureolysis and Nitrification Inhibiting Capabilities for Enhanced Nitrogen Management. *ACS Sustainable Chem. Eng.* **2019**, *7*, 13369−13378.
(40) Casali, L.; Mazzei, L.; Shemchuk, O.; Sharma, L.; Honer, K.; Grepioni, F.; Ciurli, S.; Braga, D.; Baltrusaitis, J. Novel Dual-Action Plant Fertilizer and Urease Inhibitor: Urea·Catechol Cocrystal. Characterization and Environmental Reactivity. *ACS Sustainable Chem. Eng.* **2019**, *7*, 2852−2859.
(41) Mazzeo, P. P.; Carraro, C.; Monica, A.; Capucci, D.; Pelagatti, P.; Bianchi, F.; Agazzi, S.; Careri, M.; Raio, A.; Carta, M.; Menicucci, F.; Belli, M.; Michelozzi, M.; Bacchi, A. Designing a Palette of Cocrystals Based on Essential Oil Constituents for Agricultural Applications. *ACS Sustainable Chem. Eng.* **2019**, *7*, 17929−17940.
(42) Mazzeo, P. P.; Canossa, S.; Carraro, C.; Pelagatti, P.; Bacchi, A. Systematic Coformer Contribution to Cocrystal Stabilization: Energy and Packing Trends. *CrystEngComm* **2020**, *22*, 7341−7349.
(43) Fornari, F.; Montisci, F.; Bianchi, F.; Cocchi, M.; Carraro, C.; Cavaliere, F.; Cozzini, P.; Peccati, F.; Mazzeo, P. P.; Riboni, N.; Careri, M.; Bacchi, A. Chemometric-Assisted Cocrystallization: Supervised Pattern Recognition for Predicting the Formation of New Functional Cocrystals. *Chemom. Intell. Lab. Syst.* **2022**, *226*, No. 104580.
(44) Stahly, G. P. A Survey of Cocrystals Reported Prior to 2000. *Cryst. Growth Des.* **2009**, *9*, 4212−4229.
(45) Aakeröy, C. B.; Tharanga, W.; Benton, J.; Desper, J. Stabilizing Volatile Liquid Chemicals Using Co-Crystallization. *Chem. Commun.* **2015**, *51*, 2425−2428.
(46) Capucci, D.; Balestri, D.; Mazzeo, P. P.; Pelagatti, P.; Rubini, K.; Bacchi, A. Liquid Nicotine Tamed in Solid Forms by Cocrystallization. *Cryst. Growth Des.* **2017**, *17*, 4958−4964.
(47) Bacchi, A.; Capucci, D.; Giannetto, M.; Mattarozzi, M.; Pelagatti, P.; Rodriguez-Hornedo, N.; Rubini, K.; Sala, A. Turning Liquid Propofol into Solid (without Freezing It): Thermodynamic Characterization of Pharmaceutical Cocrystals Built with a Liquid Drug. *Cryst. Growth Des.* **2016**, *16*, 6547−6555.
(48) Bacchi, A.; Mazzeo, P. P. Cocrystallization as a Tool to Stabilize Liquid Active Ingredients. *Crystallogr. Rev.* **2021**, *27*, 103−123.
(49) Aakeröy, C. B.; Beatty, A. M.; Helfrich, B. A. "Total Synthesis" Supramolecular Style: Design and Hydrogen-Bond-Directed Assembly of Ternary Supermolecules. *Angew. Chem., Int. Ed.* **2001**, *40*, 3240−3242.
(50) Braga, D.; Grepioni, F.; Maini, L.; Mazzeo, P. P.; Rubini, K. Solvent-Free Preparation of Co-Crystals of Phenazine and Acridine with Vanillin. *Thermochim. Acta* **2010**, *507−508*, 1−8.
(51) Aakeröy, C. Is There Any Point in Making Co-Crystals? *Acta Crystallogr., Sect. B: Struct. Sci., Cryst. Eng. Mater.* **2015**, *71*, 387−391.
(52) Bethune, S. J.; Schultheiss, N.; Henck, J. O. Improving the Poor Aqueous Solubility of Nutraceutical Compound Pterostilbene through Cocrystal Formation. *Cryst. Growth Des.* **2011**, *11*, 2817−2823.
(53) Babu, N. J.; Nangia, A. Solubility Advantage of Amorphous Drugs and Pharmaceutical Cocrystals. *Cryst. Growth Des.* **2011**, *11*, 2662−2679.
(54) Borrego, S.; Valdés, O.; Vivar, I.; Lavin, P.; Guiamet, P.; Battistoni, P.; Gómez de Saravia, S.; Borges, P. Essential Oils of Plants as Biocides against Microorganisms Isolated from Cuban and Argentine Documentary Heritage. *ISRN Microbiol.* **2012**, *2012*, 1−7.
(55) Solano, A. C. V.; de Gante, C. R. Two Different Processes to Obtain Antimicrobial Packaging Containing Natural Oils. *Food Bioprocess Technol.* **2012**, *5*, 2522−2528.
(56) Dorman, H. J. D.; Deans, S. G. Antimicrobial Agents from Plants: Antibacterial Activity of Plant Volatile Oils. *J. Appl. Microbiol.* **2000**, *88*, 308−316.
(57) Bassanetti, I.; Carcelli, M.; Buschini, A.; Montalbano, S.; Leonardi, G.; Pelagatti, P.; Tosi, G.; Massi, P.; Fiorentini, L.; Rogolino, D. Investigation of Antibacterial Activity of New Classes of Essential Oils Derivatives. *Food Control* **2017**, *73*, 606−612.
(58) Thozet, A.; Perrin, M. Structure of 2-Isopropyl-5-Methylphenol (Thymol). *Acta Crystallogr., Sect. B: Struct. Crystallogr. Cryst. Chem.* **1980**, *36*, 1444−1447.
(59) Braga, D.; Dichiarante, E.; Grepioni, F.; Lampronti, G. I.; Maini, L.; Mazzeo, P. P.; D'Agostino, S. Mechanical Preparation of Crystalline Materials. An Oxymoron? In *Supramolecular Chemistry*, John Wiley & Sons, Ltd: Chichester, U.K., 2012.
(60) James, S. L.; Friščić, T. Mechanochemistry. *Chem. Soc. Rev.* **2013**, *42*, 7494−7496.
(61) Braga, D.; Maini, L.; Grepioni, F. Mechanochemical Preparation of Co-Crystals. *Chem. Soc. Rev.* **2013**, *42*, 7638−7648.
(62) Gomollón-Bel, F. Ten Chemical Innovations That Will Change Our World: IUPAC Identifies Emerging Technologies in Chemistry with Potential to Make Our Planet More Sustainable. *Chem. Int.* **2019**, *41*, 12−17.

(63) Sheldrick, G. M. SHELXT-Integrated Space-Group and Crystal-Structure Determination. *Acta Crystallogr., Sect. A: Found. Adv.* **2015**, *71*, 3−8.
(64) Sheldrick, G. M. Crystal Structure Refinement with SHELXL. *Acta Crystallogr., Sect. C: Struct. Chem.* **2015**, *71*, 3−8.
(65) Dolomanov, O. V.; Bourhis, L. J.; Gildea, R. J.; Howard, J. A. K.; Puschmann, H. OLEX2: A Complete Structure Solution, Refinement and Analysis Program. *J. Appl. Crystallogr.* **2009**, *42*, 339−341.
(66) Cohen, J. Eta-Squared and Partial Eta-Squared in Fixed Factor Anova Designs. *Educ. Psychol. Meas.* **1973**, *33*, 107−112.
(67) Spackman, P. R.; Turner, M. J.; McKinnon, J. J.; Wolff, S. K.; Grimwood, D. J.; Jayatilaka, D.; Spackman, M. A. CrystalExplorer: A Program for Hirshfeld Surface Analysis, Visualization and Quantitative Analysis of Molecular Crystals. *J. Appl. Crystallogr.* **2021**, *54*, 1006−1011.
(68) Turner, M. J.; Thomas, S. P.; Shi, M. W.; Jayatilaka, D.; Spackman, M. A. Energy Frameworks: Insights into Interaction Anisotropy and the Mechanical Properties of Molecular Crystals. *Chem. Commun.* **2015**, *51*, 3735−3738.
(69) Mackenzie, C. F.; Spackman, P. R.; Jayatilaka, D.; Spackman, M. A. CrystalExplorer Model Energies and Energy Frameworks: Extension to Metal Coordination Compounds, Organic Salts, Solvates and Open-Shell Systems. *IUCrJ* **2017**, *4*, 575−587.
(70) Dovesi, R.; Orlando, R.; Erba, A.; Zicovich-Wilson, C. M.; Civalleri, B.; Casassa, S.; Maschio, L.; Ferrabone, M.; De La Pierre, M.; D'Arco, P.; Noël, Y.; Causà, M.; Rérat, M.; Kirtman, B. CRYSTAL14: A Program for the Ab Initio Investigation of Crystalline Solids. *Int. J. Quantum Chem.* **2014**, *114*, 1287−1317.
(71) Gatti, C.; Saunders, V. R.; Roetti, C. Crystal Field Effects on the Topological Properties of the Electron Density in Molecular Crystals: The Case of Urea. *J. Chem. Phys.* **1994**, *101*, 10686−10696.
(72) Grimme, S. Semiempirical GGA-Type Density Functional Constructed with a Long-Range Dispersion Correction. *J. Comput. Chem.* **2006**, *27*, 1787−1799.
(73) Aakeröy, C. B.; Beatty, A. M.; Helfrich, B. A.; Nieuwenhuyzen, M. Do Polymorphic Compounds Make Good Cocrystallizing Agents? A Structural Case Study That Demonstrates the Importance of Synthon Flexibility. *Cryst. Growth Des.* **2003**, *3*, 159−165.
(74) Vandekar, S.; Tao, R.; Blume, J. A Robust Effect Size Index. *Psychometrika* **2020**, *85*, 232−246.
(75) Groom, C. R.; Bruno, I. J.; Lightfoot, M. P.; Ward, S. C. The Cambridge Structural Database. *Acta Crystallogr., Sect. B: Struct. Sci., Cryst. Eng. Mater.* **2016**, *72*, 171−179.
(76) Desiraju, G. R. On the Presence of Multiple Molecules in the Crystal Asymmetric Unit (Z′ >1). *CrystEngComm* **2007**, *9*, 91−92.
(77) Anderson, K. M.; Steed, J. W. Comment on "On the Presence of Multiple Molecules in the Crystal Asymmetric Unit (Z′ >1)" by Gautam R. Desiraju, CrystEngComm, 2007, 9, 91. *CrystEngComm* **2007**, *9*, 328−330.
(78) Nichol, G. S.; Clegg, W. Further Thoughts on Crystal Structures with Z′ > 1: Analysis of Single-Crystal Structures Determined Using X-Ray Synchrotron and Neutron Radiation in the Cambridge Structural Database. *CrystEngComm* **2007**, *9*, 959−960.
(79) Steed, K. M.; Steed, J. W. Packing Problems: High Z′ Crystal Structures and Their Relationship to Cocrystals, Inclusion Compounds, and Polymorphism. *Chem. Rev.* **2015**, *115*, 2895−2933.
(80) Taylor, R.; Cole, J. C.; Groom, C. R. Molecular Interactions in Crystal Structures with Z′ > 1. *Cryst. Growth Des.* **2016**, *16*, 2988−3001.

https://doi.org/10.1021/acssuschemeng.2c01257
ACS Sustainable Chem. Eng. 2022, 10, 8388−8399